A Journal of the Gesellschaft Deutscher Chemiker

Angewandte International Edition

GDCh

Chemie

www.angewandte.org

Accepted Article

Title: Architecting Sub-2 nm Organosilica Nanohybrids for Far-field Super-resolution Imaging

Authors: Xiaogang Liu, Liangliang Liang, Wei Yan, Xian Qin, Xiao Peng, Feng Han, Yu Wang, Ziyu Zhu, Lingmei Liu, Yu Han, Qinghua Xu, and Junle Qu

To be cited as: *Angew. Chem. Int. Ed.* 10.1002/anie.201912404
Angew. Chem. 10.1002/ange.201912404

Link to VoR: http://dx.doi.org/10.1002/anie.201912404
http://dx.doi.org/10.1002/ange.201912404

WILEY-VCH

10.1002/anie.201912404

WILEY-VCH

Architecting sub-2 nm organosilica nanohybrids for far-field super-resolution imaging

Liangliang Liang,[a]† Wei Yan,[b]† Xian Qin,[a]† Xiao Peng,[b] Han Feng,[e] Yu Wang, [d][f] Ziyu Zhu,[a] Lingmei Liu,[c] Yu Han,[c] Qinghua Xu,[a] Junle Qu,*[b] and Xiaogang Liu*[a][d]

Abstract: Stimulated emission depletion (STED) microscopy enables ultrastructural imaging of biological samples with high spatiotemporal resolution. Herein, we report a new class of STED nanoprobes based on fluorescent organosilica nanohybrids featuring sub-2 nm size and near-unity quantum yield. Corroborated by theoretical calculations, we experimentally demonstrate that the spin-orbit coupling (SOC) effect of heavy-atom-rich organic fluorophores can be mitigated through a silane-molecule-mediated condensation/dehalogenation process, resulting in bright fluorescent organosilica nanohybrids integrating with multiple emitters in one hybrid nanodot. When harnessed as STED nanoprobes, these fluorescent nanohybrids show intense photoluminescence, high biocompatibility, and long-term photostability. By taking advantages of the low-power excitation (0.5 μW), prolonged singlet-state lifetime, and negligible depletion-induced re-excitation, these STED nanohybrids present high depletion efficiency (> 96%), extremely low saturation intensity (0.54 mW, ~0.188 MW/cm^2), and ultra-high lateral resolution of sub-20 nm (~λ_{em}/28). We believe that this approach may facilitate the expansion of the nanoprobe toolbox across imaging and biological disciplines.

Introduction

Diffraction-unlimited far-field fluorescence microscopy techniques have made a strong imprint in life sciences over the past few decades.[1] As the first fluorescence-based super-resolution imaging technique, STED microscopy has emerged as one of the most promising technologies extending our horizons to the subcellular level.[2] For a conventional STED microscopy, acquisition of subdiffractional specimen features can be realized by shrinking the active emitting region through the use of a second red-shifted donut beam. With the depletion beam, emitters in the periphery could be deexcited *via* stimulated-emission depletion and the active emitting region could be confined to the donut center. For practical STED imaging, the typical selection criteria for nanoprobes considered are small size, high fluorescent quantum yield, water solubility, biocompatibility, and photostability, as well as low saturation power required for fluorescence suppression.[3] However, it remains challenging to find a class of STED nanoprobes that fulfill all these requirements in practice. For recently emerged STED nanoprobes including, quantum dots,[4] polymer nanoparticles,[5] aggregation-induced emission nanoparticles,[6] and upconversion nanocrystals,[7] despite their distinct features, they still suffer intrinsic limitations such as large physical dimensions, high saturation intensity or low lateral resolution.

Intersystem crossing (ISC) plays a crucial role in determining the optical properties of organic fluorophores, especially for those containing heavy atoms.[8] Triggered by strong SOC, the singlet-to-triplet ISC would severely depopulate the singlet excited state and result in a drastic decrease in both the fluorescence intensity and lifetime.[9] Therefore, breaking the detrimental SOC could be a viable approach to light up fluorophores that suffering severe ISC (Figure 1a). Besides, the integration of multiple emitting centers into one nanodot could effectively enhance the emission intensity at a single-particle level.[10]

Organosilica nanomaterials have been at the forefront of biomedical research for decades.[11] Our present attempts aim at enriching the super-resolution nanoprobe toolbox with ultra-small and bright organosilica nanohybrids featuring superior super-resolution imaging performance. We choose commercially available 4,5,6,7-tetrachloro-2′,4′,5′,7′-tetraiodofluorescein as a representative organic fluorophore in support of strong SOC. In a typical experiment, through a hydrolysis-condensation/dehalogenation hydrothermal reaction mediated by (3-trimethoxysilylpropyl)diethylenetriamine in water, we obtained sub-2 nm fluorescent organosilica nanohybrids with high water solubility, biocompatibility, and ultra-high quantum yield (~ 99%). Furthermore, when serving as STED nanoprobes, these fluorescent nanohybrids showed extremely low saturation intensity (~0.54 mW, ~0.188 MW/cm^2), ultra-high lateral resolution (~19.2 nm), and high resistance to photobleaching. Our

[a] Dr. L. Liang, Dr. X. Qin, Ms. Z. Zhu, Prof. Q. Xu, and Prof. X. Liu
Department of Chemistry, National University of Singapore, Singapore 117543, Singapore
E-mail: chmlx@nus.edu.sg
[b] Dr. W. Yan, Dr. X. Peng, and Prof. J. Qu
Key Laboratory of Optoelectronic Devices and Systems of Ministry of Education and Guangdong Province, College of Optoelectronic Engineering, Shenzhen University, Shenzhen, 518060, China
E-mail: jlqu@szu.edu.sg
[c] Dr. L. Liu and Prof. Y. Han
King Abdullah University of Science and Technology, Physical Sciences and Engineering Division, Advanced Membranes and Porous Materials Center, Thuwal, Saudi Arabia
[d] Prof. Y. Wang and Prof. X. Liu
SZU-NUS Collaborative Innovation Center for Optoelectronic Science & Technology, International Collaborative Laboratory of 2D Materials for Optoelectronics Science and Technology of Ministry of Education, Institute of Microscale Optoelectronics, Shenzhen University, Shenzhen 518060, China
[e] Ms. H. Feng
Advanced Environmental Biotechnology Centre, Nanyang Environment and Water Research Institute, Interdisciplinary Graduate Programme, Nanyang Technological University, Singapore 637141, Singapore
[f] Prof. Y. Wang
Engineering Technology Research Center for 2D Material Information Function Devices and Systems of Guangdong Province, College of Optoelectronic Engineering, Shenzhen University, Shenzhen 518060, China
[†] These authors contributed equally to this work.
Supporting information for this article is given via a link at the end of the document.

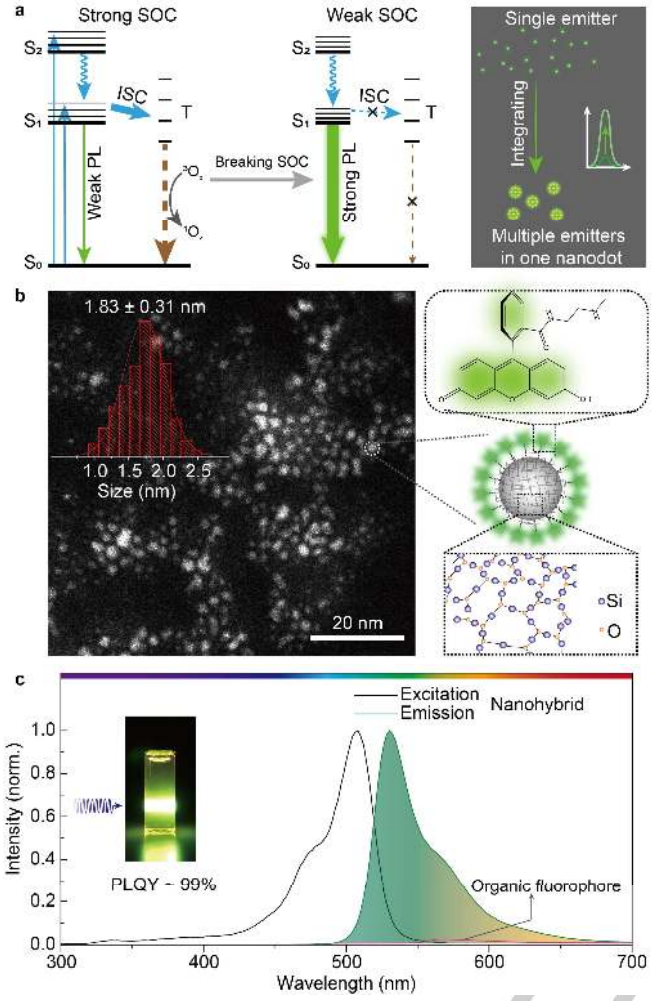

Figure 1. a) Fluorescence enhancement by breaking SOC of organic fluorophore to suppress intersystem crossing transition (left panel) and by enhancing the brightness at the single-particle level through integrating multi-emitters within one nanodot (right panel). b) STEM imaging of the obtained organosilica nanohybrids. The inset shows the size distribution of nanohybrids. The right panel illustrates that the nanohybrid consists of a crosslinked amorphous silica core with covalently attached dehalogenated dye molecular fragments. c) Fluorescence intensity comparison of the organic fluorophore under study and the as-prepared organosilica nanohybrids upon excitation at 470 nm. Inset shows a photographic image of fluorescent nanohybrids dispersed in water upon UV excitation.

experimental investigations and theoretical simulations revealed the critical role of breaking SOC in enhancing the fluorescence intensity of this new class of STED nanohybrids.

Results and Discussion

The characterization of the as-prepared fluorescent nanohybrids by scanning transmission electron microscopy (STEM) shows a mean diameter of ~ 1.83 nm (Figure 1b), which is even smaller than that of fluorescent proteins (~ 4 nm). Electron energy loss spectroscopy and energy-dispersive X-ray spectroscopy (Figure S1 a and b, Supporting Information) indicate that the process of hydrothermal dehalogenation occurs, and negligible halogen residues could be detected in dialyzed nanohybrids. Besides, the X-ray diffraction pattern reveals the amorphous silica nature of these nanohybrids (Figure S1 c, Supporting Information). Furthermore, the nonfluorescent solution obtained after thorough dialysis of nanohybrids suggests that the dehalogenated organic fluorophores are intertwined within the nanohybrids (Figure S2, Supporting Information).

Amino-rich organosilica nanodots could be obtained through the hydrothermal treatment of the silane precursor alone, and the amide group formed upon addition of the organic fluorophore (Figure S3, Supporting Information). Therefore, these fluorescent nanohybrids are likely composed of organosilica cores with covalently linked multi-emitting centers. This structural arrangement enables access to ultra-small size while retaining high brightness in a single nanodot.

In addition to the excellent aqueous stability for several months (Figure S4, Supporting Information), the as-obtained organosilica nanohybrids, upon blue light illumination, showed broadband (~ 500 nm to 650 nm) emission with a near-unity fluorescence quantum yield of ~ 99% (Figure 1c; Figure S5a, Supporting Information). Contrastingly, the aqueous solution of the original fluorophore showed a weak emission with intensity being only 2% of its nanohybrid counterpart (Figure S5b, Supporting Information). Notably, without the assistance of the silane molecules, a turbid solution with unnoticeable fluorescence intensification was obtained under the same experimental condition (Figure S6, Supporting Information). Given the susceptibility of phosphorescence to oxygen and the dehalogenation process, we argue that such luminescence enhancement detected in the nanohybrids could mainly be ascribed to the effective suppression of singlet-to-triplet intersystem crossing.

To validate this hypothesis, we measured the luminescence of organic fluorophore and nanohybrids dispersed in glycerol/water mixtures with gradient controls over solvent viscosities and dissolved oxygen contents (Figure S7, Supporting Information).[12] In the case of pure organic fluorophore, we found that the phosphorescence from the triplet radiative decay starts emerging and increases rapidly when decreasing the water concentration (Figure 2a). This phenomenon suggests an alleviation in oxygen-induced triplet-state quenching, as corroborated by the observation of drastically prolonged phosphorescence lifetime (Figure 2b, Figure S8 a, Supporting Information). In addition, luminescence from the singlet state is also strengthened, accompanied by an increase in the fluorescence lifetime from 0.12 to 0.53 ns (Figure 2b, Figure S8b, Supporting Information). This amplification occurs most likely because of the effective mitigation in solvent molecular vibration since the singlet-state fluorescence is insensitive to the dynamic collisional quenching from dissolved oxygen. In sharp contrast, the nanohybrids do not show any phosphorescence, even when water is completely replaced by glycerol (Figure 2c). Surprisingly, the phosphorescence of the nanohybrids could not be detected even in liquid nitrogen, even though a low-temperature is likely to boost the phosphorescence from a pure organic fluorophore (Figure S9, Supporting Information). Therefore, we believe that the unfavorable SOC in organosilica nanohybrids is largely suppressed, which in turn effectively blocks the pathway of fluorescence quenching through the singlet-to-triplet transition. For organosilica nanohybrids dispersed in pure water, a more than 36-fold prolonged fluorescence lifetime of 4.37 ns was

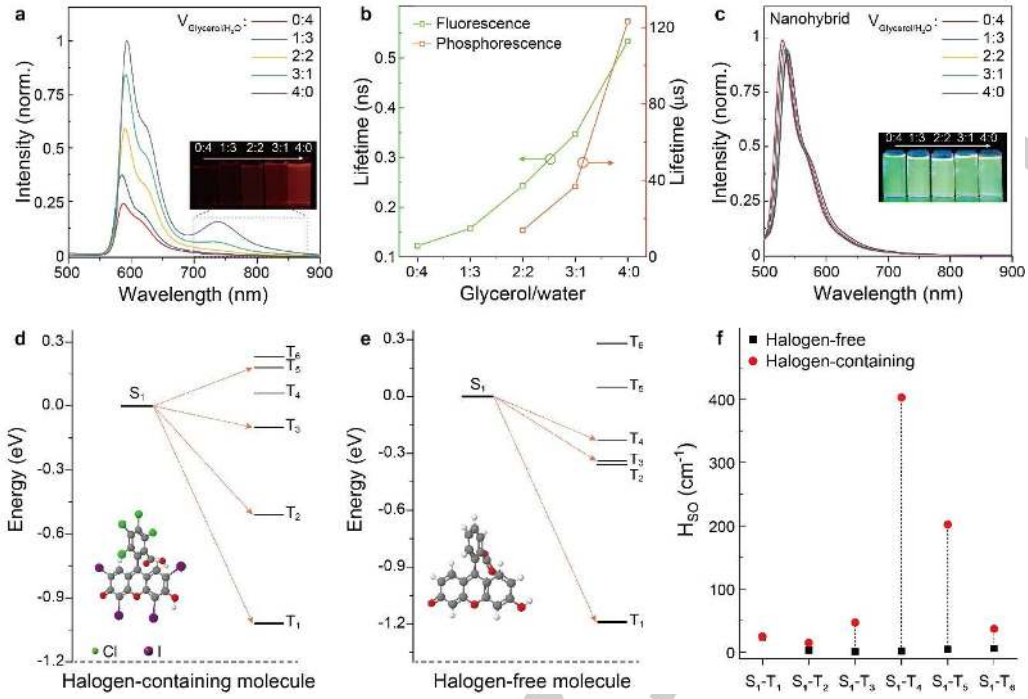

Figure 2. a) Luminescence intensity variation of organic fluorophore dispersed in water solutions with different volume ratios of glycerol. Insets are the corresponding photographic images upon 365 nm LED excitation with a 700 nm-long pass filter. b) Fluorescence and phosphorescence lifetimes of heavy-atom rich organic fluorophore dispersed in glycerol/water solutions. c) Fluorescence spectra and corresponding images of the nanohybrids dispersed in mixture solutions. Schematic diagrams showing the TD-DFT-calculated energy levels of d) the heavy-atom enriched and e) dehalogenated organic fluorophore. f) Calculated SOC parameters in the Hamiltonian between the lowest excited singlet state and excited triplet states for the organic fluorophore before and after dehalogenation.

observed (Figure S10, Supporting Information). Interestingly, the fluorescence intensity from these nanohybrids shows negligible change upon addition of glycerol, indicating that the emitting centers are integrated into these nanohybrids in a rigidified form with high resistance to solvent-associated quenching (Figure 2c).[13]

To shed more light on the mechanism of the enhanced fluorescence from the nanohybrids, we performed *ab-initio* investigations, through the use of time-dependent density functional theory (TDDFT)[14] on the singlet and triplet excited states of the organic fluorophores before and after dehalogenation. By analyzing the energy gap between the lowest singlet excited state and other triplet excited states, we found significant energy gaps between S_1 and T_1 excited states (over 1.0 eV) for both the halogen-containing and halogen-free molecules, thus indicating a noneffective intersystem crossing via $S_1 \rightarrow T_1$ channel (Figure 2d and 2e). On the other hand, when compared with the S_1-T_1 gap, the gap between S_1 state and higher triplet states such as T_2 and T_3 becomes smaller in both molecular systems. Notably, the calculated S_1 and T_3 energy levels of the halogen-containing molecule have a small gap of ~ 0.1 eV, which facilitates the singlet-to-triplet intersystem crossing. Moreover, the matched orbital transition components between S_1 and higher triplet states in these two molecules confirm the intersystem crossing from S_1 state to multiple triplet states (Table S1 and S2, Supporting Information). In addition to the aforementioned energy gap, the spin-orbital coupling between singlet and triplet excited states also plays a crucial role in determining the efficiency of the intersystem crossing. For the S_1-T_1 spin-orbital coupling, we found a comparable spin-orbital coupling parameter of ~25 cm^{-1} for both molecules. However, the S_1-(T_3, T_4, or T_5) spin-orbital coupling parameter in the halogen-free molecule is much smaller than that of the halogen-containing molecule (Figure 2f). Given the large gap combined with low spin-orbital coupling, the process of intersystem crossing is significantly suppressed in the halogen-free molecule, which is in line with the enhanced fluorescence observed for the nanohybrids.

In a further set of experiment , we evaluated the performance of the as-prepared organosilica nanohybrids in STED imaging (Figure S11, Supporting Information). As shown in Figure 3a, upon 488 nm excitation, the luminescence intensity of the nanohybrids declined rapidly with increase in the STED power (P_{STED}) of a continuous-wave (CW) depletion beam at 660 nm, and more than 90% of the initial luminescence could be suppressed when P_{STED} was set at 10 mW. When applying the depletion beam alone, no distinguishable fluorescence from the nanohybrids was detectable, and a depletion efficiency of ~ 96% could be achieved with a P_{STED} of 38 mW. Furthermore, the average full-width-at-half-maximums (FWHMs), calculated from the imaging data, were plotted as a function of P_{STED}, and the data were fitted using the theoretical resolution formula for STED microscopy[4b]. As indicated in Figure 3b, the effective spot size of the nanohybrids shrank drastically, and a resolution around 60 nm could be achieved using a depletion power of only 5 mW. Notably, an ultra-low saturation power (P_{sat}) of 0.54 mW (~0.188 MW/cm^2) was determined, which is much lower than that of commercially available quantum dots and organic biomarkers.[4b, 15] The optical diffraction limitation associated with confocal microscopy imaging could be easily overcome by our nanohybrid-based STED imaging, as evidenced by the visualization of clearly resolved

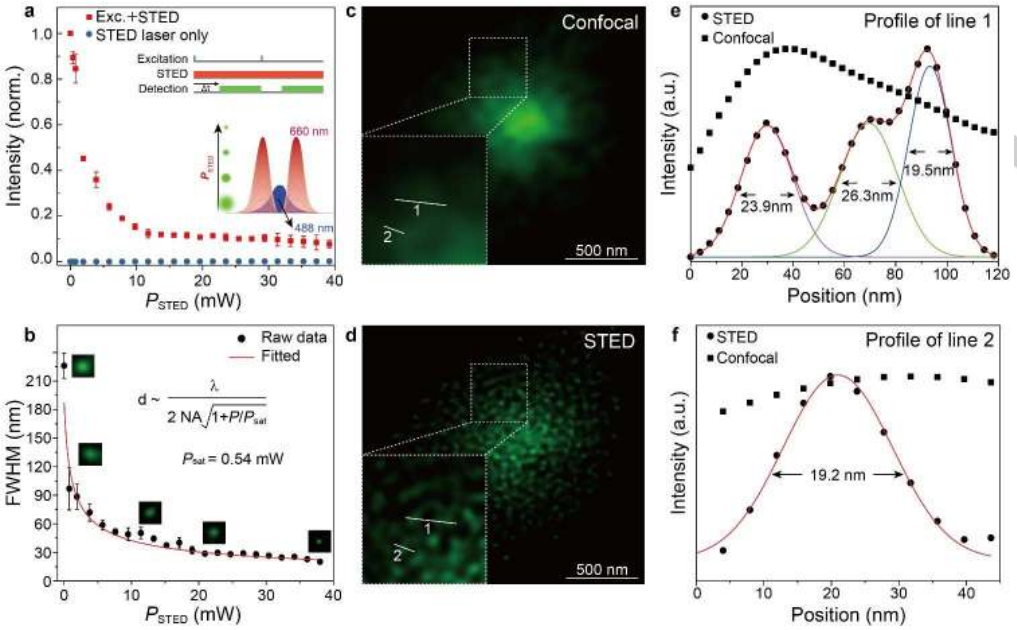

Figure 3. a) Stimulated emission depletion efficiency of the organosilica nanohybrids upon a 488 nm Gaussian beam excitation and a 660 nm donut beam depletion at varied depletion powers. The inserted illustrates the timing scheme for time-gated STED microscopy operated with a CW-STED beam and the shrinking of active emitting region upon an increase in the P_{STED}. Here the excitation power is fixed at 0.5 μW. b) Lateral-resolution variation of STED images obtained at increased P_{STED} for nanohybrids. c) Confocal microscopy imaging upon 488 nm excitation (0.5 μw) and d) corresponded STED microscopy imaging with an additional depletion beam (38 mW). e) and f) Fluorescence intensity profiles along line 1 and 2 in c) and d), respectively.

discrete spots (Figure 3, c and d). According to the corresponded line profiling (Figure 3, e and f), the use of these fluorescent nanohybrids enables access to an ultra-high lateral resolution of ~19.2 nm; this represents a more than ten-fold resolution improvement.

Cancer cells were found to effectively uptake prepared organosilica nanohybrids via endocytosis and possible passive diffusion (Figure S12, Supporting Information), and the toxicity of these nanohybrids is negligible (Figure S13, Supporting Information). Thus, Hela cells treated with fluorescent organosilica nanohybrids were imaged using confocal microscopy and STED microscopy to demonstrate the potential of these nanohybrids for super-resolution bioimaging (Figure 4a). It could be found that the nanohybrids could stain the Hela cells uniformly. However, in the conventional microscopy image, restricted by the resolution limit (~ 286 nm), sharp pictures of closely spaced point objects could not be resolved. In contrast, as profiled in Figure 4b, the organosilica nanohybrid-mediated STED microscopy imaging could provide more details and a lateral resolution of ~ 43.6 nm is achievable at a low depletion power of 18 mW. Besides, these fluorescent organosilica nanohybrids show high resistance to photobleaching (Figure S14, Supporting Information). As shown in Figure 4c, after a continuous acquisition of 100 frames, the STED image remains about 50 % of its initial intensity with a brightness adequate to identify subdiffraction features, indicating their potential for time-lapse super-resolution imaging.

Conclusion

In conclusion, we have developed a new class of STED nanoprobe based on organosilica nanohybrids. Through a silane-mediated hydrolysis condensation/dehalogenation process, it is possible to integrate multiple emitters within a single fluorescent nanoparticle, and the ISC induced by SOC could be efficiently alleviated. As approaches to controlling the emission of these nanohybrids in the near-infrared region further develop, a more coherent growth of their utility in relation to analytical applications may be anticipated. Apart from super-resolution optical imaging, this new class of fluorescent nanohybrids may find use in other emerging fields, including single-molecule tracking, subcellular pH sensing, visualization of intra-neuronal motor protein transport[16], and potentially many others.

Acknowledgements

This work is supported by the Singapore Ministry of Education (MOE2017-T2-2-110), Agency for Science, Technology and Research (A*STAR) (Grant NO. A1883c0011), National Research Foundation, Prime Minister's Office, Singapore under its Competitive Research Program (Award No. NRF-CRP15-2015-03) and under the NRF Investigatorship programme (Award No. NRF-NRFI05-2019-0003), the National Key R&D Program of China (2017YFA0700500), the National Natural Science Foundation of China (21771135, 21701119, 61705137, 81727804, 61975127), the Science and Technology Project of Shenzhen (KQJSCX20180328093614762). The computational work for this article was supported by resources of the Hihg Performance Co mputing System at National University of Singapore.

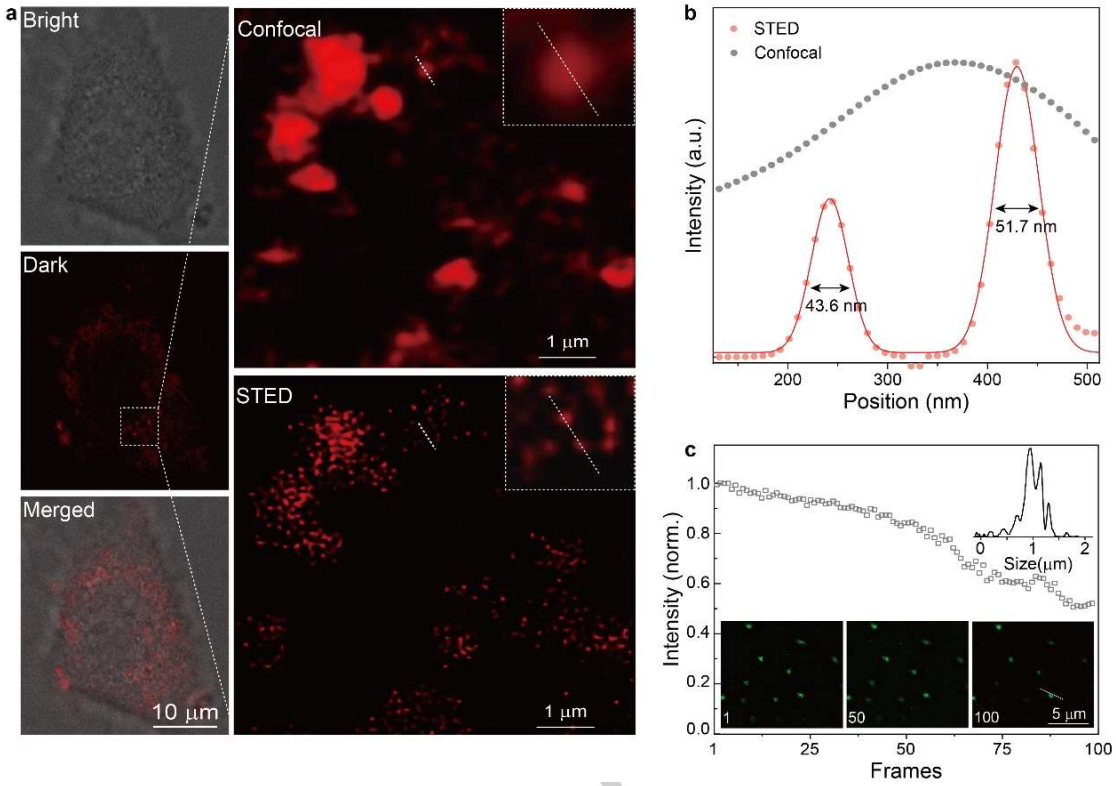

Figure 4. a) Comparison of fluorescent organosilica nanohybrid-mediated confocal microscopy and STED microscopy imaging of Hela cells with excitation laser of 0.5 μW at 488 nm and STED laser of 18 mW at 660 nm. b) Fluorescence intensity profiles along the dashed lines across the nanohybrids in a). c) Normalized STED imaging fluorescence intensity of nanohybrids against the number of frames under continuous scanning with an excitation power of 0.5 μW and STED power of 18 mW. Insets: STED microscopy imaging of fluorescent nanohybrids taken at selected frames (frame-1,50, and 100) and the intensity profile along the dashed line in frame-100.

Conflict of interest

The authors declare no conflict of interest.

Keywords: organosilica nanohybrids • spin-orbital coupling • stimulated emission depletion microscopy• super-resolution imaging

[1] a) E. Betzig, G. H. Patterson, R. Sougrat, O. W. Lindwasser, S. Olenych, J. S. Bonifacino, M. W. Davidson, J. Lippincott-Schwartz, H. F. Hess, *Science* **2006**, *313*, 1642-1645; b) K. I. Willig, R. R. Kellner, R. Medda, B. Hein, S. Jakobs, S. W. Hell, *Nat. Methods* **2006**, *3*, 721; c) M. Bates, B. Huang, G. T. Dempsey, X. Zhuang, *Science* **2007**, *317*, 1749-1753; d) B. Huang, W. Wang, M. Bates, X. Zhuang, *Science* **2008**, *319*, 810-813; e) E. Rittweger, K. Y. Han, S. E. Irvine, C. Eggeling, S. W. Hell, *Nat. Photonics* **2009**, *3*, 144; f) B.-C. Chen, W. R. Legant, K. Wang, L. Shao, D. E. Milkie, M. W. Davidson, C. Janetopoulos, X. S. Wu, J. A. Hammer, Z. Liu, *Science* **2014**, *346*, 1257998; g) F. Balzarotti, Y. Eilers, K. C. Gwosch, A. H. Gynnå, V. Westphal, F. D. Stefani, J. Elf, S. W. Hell, *Science* **2017**, *355*, 606-612; h) S. Letschert, A. Göhler, C. Franke, N. Bertleff-Zieschang, E. Memmel, S. Doose, J. Seibel, M. Sauer, *Angew. Chem. Int. Ed.* **2014**, *53*, 10921-10924; *Angew. Chem.* **2014**, *126*, 11101– 11104. i) T. Schlichthaerle, M. T. Strauss, F. Schueder, A. Auer, B. Nijmeijer, M. Kueblbeck, V. Jimenez Sabinina, J. V. Thevathasan, J. Ries, J. Ellenberg, R. Jungmann, *Angew. Chem. Int. Ed.* **2019**, *58*, 13004-13008; *Angew. Chem.* **2019**, *131*, 13138– 13142. j) W. E. Moerner, *Angew. Chem. Int. Ed.* **2015**, *54*, 8067-8093; *Angew. Chem.* **2015**, *127*, 8182-8210.

[2] a) S. W. Hell, J. Wichmann, *Opt. Lett.* **1994**, *19*, 780-782; b) S. W. Hell, *Science* **2007**, *316*, 1153-1158; c) C. Eggeling, C. Ringemann, R. Medda, G. Schwarzmann, K. Sandhoff, S. Polyakova, V. N. Belov, B. Hein, C. Von Middendorff, A. Schönle, *Nature* **2009**, *457*, 1159; d) V. Westphal, S. O. Rizzoli, M. A. Lauterbach, D. Kamin, R. Jahn, S. W. Hell, *Science* **2008**, *320*, 246-249; e) T. A. Klar, S. W. Hell, *Opt. Lett.* **1999**, *24*, 954-956; f) R. J. Kittel, C. Wichmann, T. M. Rasse, W. Fouquet, M. Schmidt, A. Schmid, D. A. Wagh, C. Pawlu, R. R. Kellner, K. I. Willig, *Science* **2006**, *312*, 1051-1054; g) R. S. Erdmann, H. Takakura, A. D. Thompson, F. Rivera‐Molina, E. S. Allgeyer, J. Bewersdorf, D. Toomre, A. Schepartz, *Angew. Chem. Int. Ed.* **2014**, *53*, 10242-10246; *Angew. Chem.* **2014**, *126*, 10407-10412.

[3] H. Blom, J. Widengren, *Chem. Rev.* **2017**, *117*, 7377-7427.

[4] a) S. Ye, W. Yan, M. Zhao, X. Peng, J. Song, J. Qu, *Adv. Mater.* **2018**, *30*, 1800167; b) J. Hanne, H. J. Falk, F. Görlitz, P. Hoyer, J. Engelhardt, S. J. Sahl, S. W. Hell, *Nat. Commun.* **2015**, *6*, 7127.

[5] Y. Wu, H. Ruan, R. Zhao, Z. Dong, W. Li, X. Tang, J. Yuan, X. Fang, *Adv. Opt. Mater.* **2018**, *6*, 1800333.

[6] D. Li, W. Qin, B. Xu, J. Qian, B. Z. Tang, *Adv. Mater.* **2017**, *29*, 1703643.

[7] a) Y. Liu, Y. Lu, X. Yang, X. Zheng, S. Wen, F. Wang, X. Vidal, J. Zhao, D. Liu, Z. Zhou, C. Ma, J. Zhou, J. A. Piper, P. Xi, D.

Jin, *Nature* **2017**, *543*, 229; b) Q. Zhan, H. Liu, B. Wang, Q. Wu, R. Pu, C. Zhou, B. Huang, X. Peng, H. Ågren, S. He, *Nat. Commun.* **2017**, *8*, 1058.

[8] a) S. McGlynn, J. Daigre, F. Smith, *J. Chem. Phys.* **1963**, *39*, 675-679; b) A. Horrocks, A. Kearvell, K. Tickle, F. Wilkinson, *Trans. Faraday Society* **1966**, *62*, 3393-3399; c) H. Shizuka, M. Nakamura, T. Morita, *J. Phys. Chem.* **1980**, *84*, 989-994; d) W. Zhao, Z. He, Q. Peng, J. W. Lam, H. Ma, Z. Qiu, Y. Chen, Z. Zhao, Z. Shuai, Y. Dong, *Nat. Commun.* **2018**, *9*, 3044;

[9] a) J. C. Koziar, D. O. Cowan, *Acc. Chem. Res.* **1978**, *11*, 334-341; b) E. l. G. Azenha, A. C. Serra, M. Pineiro, M. M. Pereira, J. S. de Melo, L. G. Arnaut, S. J. Formosinho, R. G. AMd'A, *Chem. Phys.* **2002**, *280*, 177-190; c) M. N. B. Santos, *PhysChemComm* **2000**, *3*, 18-23; d) P. K. Samanta, D. Kim, V. Coropceanu, J.-L. Brédas, *J. Am. Chem. Soc.* **2017**, *139*, 4042-4051.

[10] a) D. Jin, P. Xi, B. Wang, L. Zhang, J. Enderlein, A. M. van Oijen, *Nat. Methods* **2018**, *15*, 415; b) S. Wen, J. Zhou, K. Zheng, A. Bednarkiewicz, X. Liu, D. Jin, *Nat. Commun.* **2018**, *9*, 2415; c) L. Liang, D. B. Teh, N.-D. Dinh, W. Chen, Q. Chen, Y. Wu, S. Chowdhury, A. Yamanaka, T. C. Sum, C.-H. Chen, *Nat. Commun.* **2019**, *10*, 1391; d) L. Liang, X. Qin, K. Zheng, X. Liu, *Acc. Chem. Res.* **2019**, *52*, 228-236. e) X. Qin, J. Xu, Y. Wu, X. Liu, *ACS Cent. Sci.* **2019**, *5*, 29-42.

[11] a) J. G. Croissant, Y. Fatieiev, A. Almalik, N. M. Khashab, *Adv. Healthcare Mater.* **2018**, *7*, 1700831; b) Z. Teng, W. Li, Y. Tang, A. Elzatahry, G. Lu, D. Zhao, *Adv. Mater.* **2018**, 1707612; c) L. Yu, Y. Chen, H. Lin, W. Du, H. Chen, J. Shi, *Biomaterials* **2018**, *161*, 292-305; d) X. Chen, X. Zhang, L.-Y. Xia, H.-Y. Wang, Z. Chen, F.-G. Wu, *Nano Lett.* **2018**, *18*, 1159-1167; e) T. Himiyama, M. Waki, Y. Maegawa, S. Inagaki, *Angew. Chem. Int. Ed.* **2019**; *Angew. Chem.* **2019**, *131*, 9248-9252; f) E. A. Prasetyanto, A. Bertucci, D. Septiadi, R. Corradini, P. Castro‐Hartmann, L. De Cola, *Angew. Chem. Int. Ed.* **2016**, *55*, 3323-3327; *Angew. Chem.* **2016**, *128*, 3292-3292

[12] a) C. Parker, C. Hatchard, *Trans. Faraday Society* **1961**, *57*, 1894-1904; b) M. L. Saviotti, W. C. Galley, *Proc. Natl. Acad. Sci. U. S. A.* **1974**, *71*, 4154-4158.

[13] Z. Wei, Z.-Y. Gu, R. K. Arvapally, Y.-P. Chen, R. N. McDougald Jr, J. F. Ivy, A. A. Yakovenko, D. Feng, M. A. Omary, H.-C. Zhou, *J. Am. Chem. Soc.* **2014**, *136*, 8269-8276.

[14] M. Petersilka, U. J. Gossmann, E. K. U. Gross, *Phys. Rev. Lett.* **1996**, *76*, 1212-1215.

[15] M. D. Bordenave, F. Balzarotti, F. D. Stefani, S. W. Hell, *J. Phys. D: Appl. Phys.* **2016**, *49*, 365102.

[16] X. Zeng, S. Chen, A. Weitemier, S. Han, A. Blasiak, A. Prasad, K. Zheng, Z. Yi, B. Luo, I.-H. Yang, N. Thakor, C. Chai, K.-L. Lim, T. J. McHugh, A. H. All, X. Liu, *Angew. Chem. Int. Ed.* **2019**, *58*, 9262-9268; *Angew. Chem.* **2019**, *131*, 9363-9369

10.1002/anie.201912404

WILEY-VCH

Entry for the Table of Contents

RESEARCH ARTICLE

A new class of nanoprobe for stimulated emission depletion (STED) microscopy imaging was developed using ultra-small and bright fluorescent organosilica nanohybrids featuring low saturation intensity, high depletion efficiency, and sub-20 nm lateral resolution.

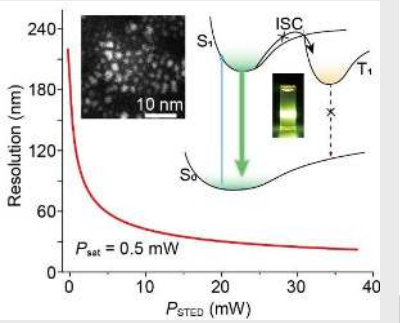

Liangliang Liang, Wei Yan, Xian Qin, Xiao Peng, Han Feng, Yu Wang, Ziyu Zhu, Lingmei Liu, Yu Han, Qinghua Xu, Junle Qu, and Xiaogang Liu**

Page No. – Page No.

Architecting sub-2 nm organosilica nanohybrids for far-field super-resolution imaging